#### **CONFERENCE PRE-PRINT**

# THREE-DIMENSIONAL NONLINEAR MODELLING OF ELM DYNAMICS WITH BIASING IN HL-3 TOKAMAK

J. Huang, G. Z. Hao, J. X. Li, Z. J. Li, T. F. Sun, B. T. Cui, H. K. Yin, L. Wang, H. Z. Zhao, X. Q. Ji, W. L. Zhong Southwestern Institute of Physics

Chengdu, China

Email: huangjie@swip.ac.cn, haogz@swip.ac.cn

Y. Suzuki

Graduate School of Advanced Science and Engineering, Hiroshima University Higashi-Hiroshima, Japan

Y. Q. Liu General Atomics San Diego, United States of America

Y. Liang

Forschungszentrum Jülich GmbH, Institute of Fusion Energy and Nuclear Waste Management Jülich, Germany

#### Abstract

The influence of a biased divertor target system on Edge Localized Mode (ELM) dynamics is investigated for the first time in the HL-3 tokamak, focusing on the impact of bias-driven scrape-off layer (SOL) helical currents on three-dimensional (3D) magnetohydrodynamic (MHD) equilibria and instabilities. In a designed 1.6 MA H-mode discharge scenario, the applied SOL currents are modelled as filamentary currents aligned with magnetic field lines near the separatrix, and the resulting 3D perturbed magnetic fields are computed using Biot–Savart law. Nonlinear resistive equilibrium simulations with the HINT code show that the bias-driven currents significantly alter the pressure distribution and magnetic topology near resonant rational surfaces and in the edge stochastic layers, particularly in the pedestal region. Subsequent 3D nonlinear MHD analysis using the MIPS code reveals that the growth rate of edge MHD instabilities systematically decreases with increasing SOL current, with a marked reduction observed at 1 kA. Additionally, nonlinear interactions between the external perturbations and intrinsic ballooning modes lead to a redistribution of the mode energy. These results demonstrate the potential of divertor biasing as a viable technique for ELM control in HL-3, offering a promising strategy for controlling edge instabilities and managing heat flux distribution in mega-ampere plasma current H-mode scenarios.

#### 1. INTRODUCTION

Edge Localized Modes (ELMs) are MHD events that occur in the edge region of a tokamak plasma during High-confinement mode (H-mode) [1], characterized by periodic collapses of the edge pedestal. Each ELM burst is associated with expulsion of large amounts of heat and particles onto the plasma-facing components. The intolerable transient heat loads may ablate the plasma-facing components like divertor plates, leading to a strong reduction of the lifetime [2]. In addition, ELMs might potentially couple or trigger other instabilities, such as the resistive wall mode [3] and the neoclassical tearing mode [4]. The prevention or control of type-I ELMs in H-mode plasma is a big issue for the next generation of fusion devices like ITER [5].

A promising method for ELM control is the application of Resonant Magnetic Perturbations (RMPs) [6]. These perturbations, generated by specially designed coils, have demonstrated their effectiveness on various devices such as DIII-D [7], JET [8], MAST [9], ASDEX-Upgrade [10], KSTAR [11] and EAST [12]. These experimental findings have positioned RMPs as one of the most promising approaches for ELM control in ITER [13]. RMP penetration can induce magnetic islands on resonant rational surface where q = m/n, with q being the safety factor and m, n the poloidal and toroidal mode numbers, respectively. When island chains on adjacent rational surfaces overlap, the magnetic field lines become chaotic. Due to the strong magnetic shear at the plasma edge in divertor configuration with an X-point, island overlap can occur readily, leading to stochastic magnetic field behaviour. This stochasticity degrades the edge transport barrier, keeping the plasma in a stable regime with respect to the peeling-ballooning mode [14]. Nevertheless, installing and utilizing RMP coils in a fusion reactor environment is challenging due to space constraints and high neutron fluxes. In parallel, the concept of magnetic perturbations generated by toroidally non-axisymmetric currents in the SOL plasma, induced by biased divertor plates, has been proposed both theoretically and experimentally, notably in devices like HL-2A [15]. Since the

helix of magnetic field lines in the SOL region is close to that in the pedestal region during H-mode, SOL currents aligned with the magnetic field near the plasma edge can also induce resonant magnetic perturbations, leading to changes in edge magnetic topology and modifications to ELM behaviour. Recently, a divertor biased target system has been designed for the HL-3 tokamak to explore the effects of divertor induced SOL current on plasma behaviour. The potential of this biased system for ELM control in H-mode discharges with mega-ampere plasma current should be investigated through modelling.

The modelling of ELM dynamics commonly relies on nonlinear MHD formulations, and several numerical codes have been developed over the past three decades, including JOREK [16], BOUT++ [17], M3D [18], NIMROD [19], MEGA [20]. In this paper, to investigate magnetic perturbations effects on ELM dynamics with 3D MHD equilibrium in finite- $\beta$  plasmas (where  $\beta$  denotes the ratio of plasma pressure to magnetic pressure), the nonlinear MHD code MIPS [21], in combination with the HINT code [22], is employed.

The paper is organized as follows. Section 2 introduces the modelling approach for simulating ELM dynamics with a divertor-based target system. Section 3 presents the analysis of 3D MHD equilibrium and ELM behaviour with bias-driven SOL current. Conclusions and discussions are provided in Section 4.

#### 2. NUMERICAL SCHEME

The flowchart of the ELM dynamics simulation with biasing is shown in Fig. 1 (a). The initial two-dimensional (2D) plasma equilibrium is generated using OMFIT [23], based on a 1.6 MA discharge featuring a H-mode pedestal structure and an upper single null (USN) configuration, which provides the 2D plasma parameters for the subsequent analysis. Starting from the 2D magnetic field, a field-line tracing method is applied to simulate the SOL current filaments driven by the external biasing system. Given the biasing configuration and current filaments, the resulting 3D magnetic perturbations are calculated using Biot–Savart law. To optimize the configuration, the resulting resonant magnetic perturbation spectrum and the associated magnetic topology in the flux (PEST) coordinate are analysed. Following the identification of a suitable biasing setup, the impact of the SOL current amplitude on the 3D MHD equilibrium is investigated using the HINT code. Finally, the nonlinear evolution of ELM dynamics is simulated with the MIPS code.

The HINT code solves the 3D nonlinear equilibrium by a two-step relaxation method on a rectangular grid in cylindrical coordinate  $(R, \phi, Z)$ , where R and Z denote the horizontal and the vertical directions, respectively, and  $\phi$  is the toroidal angle. In the presented simulation, the grid resolution is set to  $512 \times 128 \times 1024$  in the R,  $\phi$  and Z directions. The initial conditions are constructed by superposing the 2D equilibrium pressure, plasma current, and magnetic field with the 3D perturbations generated by the biasing system. Without assuming nested flux surfaces, HINT enables accurate resolution of 3D MHD equilibrium including magnetic islands and stochastic regions. The plasma equilibrium response and the modified magnetic topology are self-consistently obtained upon relaxation to the final 3D equilibrium with the applied biasing in a finite- $\beta$  plasma.

The MIPS code solves the full set of MHD equations in the same cylindrical coordinates as HINT, employing a finite difference method. Initialized with the equilibrium output, time integration is performed via a fourth-order Runge–Kutta scheme to enable the simulation of MHD dynamics through time evolution. In the simulation, the resistivity follows the Spitzer model, scaling with temperature as  $T^{-3/2}$ . To minimize the influence of artificial boundary effects on edge instabilities, the plasma domain in MIPS is extended slightly beyond the first wall.

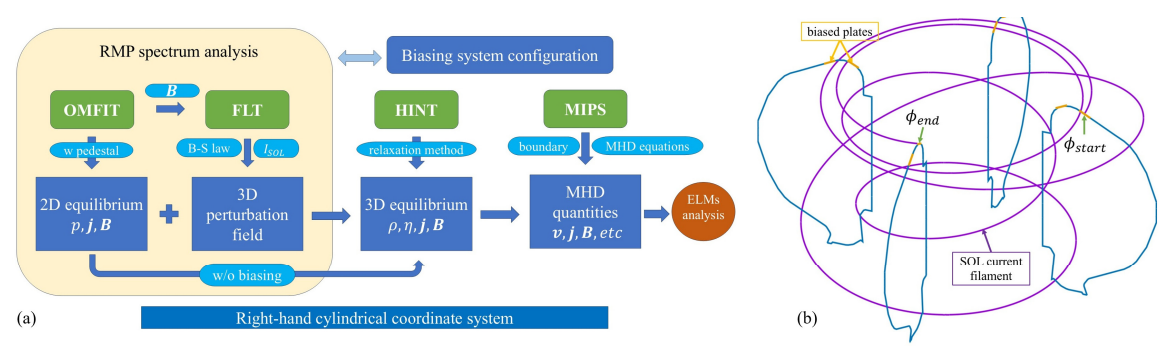


FIG. 1. (a) Flowchart of the ELM dynamics simulation process with biasing. (b) 3D view of the bias-driven SOL current filament indicated by the thick purple line. The biased plate locations are marked along the orange line.

#### 3. NUMERICAL RESULTS

#### 3.1. Biasing configuration with RMP spectrum analysis

An upper divertor biased target system has been designed with four groups of biasing plates in HL-3. As shown in Fig. 1 (b), there are eight biasing plates located on the upper first wall, with four positioned on the inner side and four on the outer side, uniformly distributed in the toroidal direction. When both the start and end points of a bias-driven SOL current filament are constrained to the biased plates, three representative biasing configurations can be defined: '+0-0', '++-'and '+-+'. Here '+' denotes a current flowing from the outer to the inner plate (equivalently, a positive bias applied to the outer plate), '-' denotes the opposite direction, and '0' indicates that no bias is applied at that plate. The first two configurations correspond to n=1 dominant magnetic perturbations, while the latter correspond to n=2. Other possible configurations, such as '+00' and '+0+0', are also feasible but produce comparatively weaker resonant effects.

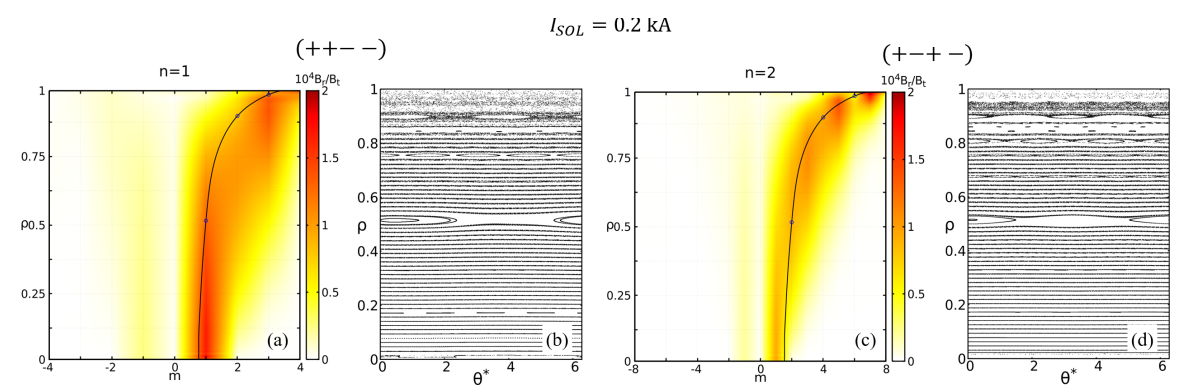


FIG. 2. (a), (c) Resonant component spectra and (b), (d) Poincaré plots in PEST coordinates for the '++--' and '+-+-' configurations. The black curve represents the safety factor q profile, with blue circles marking the q=1, 2, and 3 rational surfaces.

To determine an appropriate biasing configuration for subsequent nonlinear simulations, the vacuum RMP spectrum and associated magnetic topology are analysed. The results indicate that configurations involving a greater number of biased plates produce stronger RMPs at a fixed SOL current amplitude. For instance, in the n=1 dominant case, the '+ + - -' configuration exhibits a stronger resonant spectrum than the '+ 0 0 0' or '+ 0 - 0' cases. Fig. 2 presents the RMP spectra and corresponding Poincaré plots for the '+ + - -' and '+ - + -' configurations, both with a bias-driven SOL current of  $I_{SOL}=0.2$  kA. While the two configurations show similar resonant strengths near the edge, the '+ + - -' case exhibits a slightly enhanced resonant amplitude in the core region. This is reflected in the magnetic island width at the q=1 surface, which scales with the square root of the resonant magnetic field amplitude at the corresponding rational surface, i.e.  $\sqrt{B_{\rm r_{m,n}}}$  and is marginally larger in the '+ + - -' case. The level of edge stochasticity is comparable between the two. To ensure adequate edge resonance for modifying the pedestal topology while limiting core perturbations and preserving overall confinement, the '+ - + -' configuration is selected as the optimal choice for subsequent nonlinear simulations. It is also noted that, in contrast to conventional 3D RMP coils which produce both resonant and non-resonant ( $\pm m$ , n) harmonics, the bias-driven helical SOL currents aligned with magnetic field lines predominantly generate (m, n) components, effectively suppressing non-resonant contributions or the kink effects.

# 3.2. Three-Dimensional equilibrium with biasing

Based on the '+ - + -' configuration, 3D nonlinear resistive MHD equilibria are calculated with the HINT code for a range of bias-driven SOL current amplitudes. As the perturbated field superimposed, magnetic islands form and the edge magnetic field becomes increasingly stochastic. The pressure profile evolves self-consistently to satisfy the dynamic force balance equation  $\vec{J} \times \vec{B} = \nabla p$ . Fig. 3 presents a comparison of equilibrium pressure distributions with a bias-driven SOL current of  $I_{\text{SOL}} = 0.2 \text{ kA}$  across selected toroidal cross-sections, highlighting the 3D structure and significant modifications of edge region. Owing to the n = 2 dominant biasing configuration, the resulting pressure and magnetic topology at  $\phi = 0$  and  $\phi = \pi$  are qualitatively similar. It should be noted that in the Poincaré plots, certain magnetic islands are not fully resolved due to the uniform seeding of field-line tracing points from the magnetic axis to the X-point. For example, the (m, n) = (2,2) magnetic island chain near the original q = 1 surface appears partially incomplete (only one island is visible in

the plot near the core), as the two islands reside in separate flux tubes under n = 2 dominant resonant perturbations.

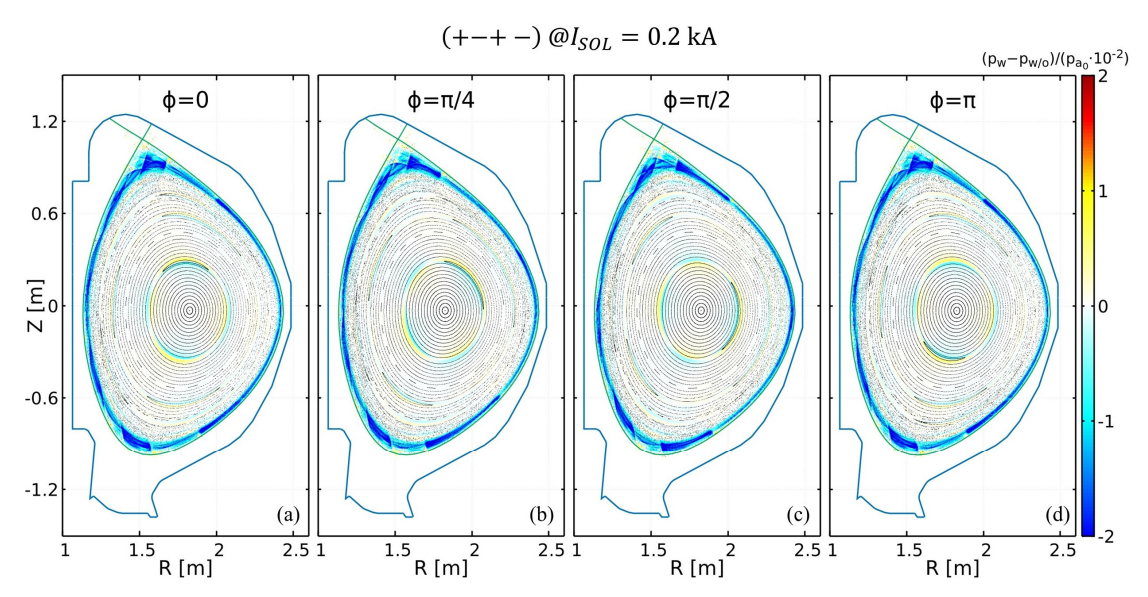


FIG. 3. (a), (c) Pressure modifications and Poincaré plots in cylindrical coordinates at selected toroidal cross-sections for the '+ - + -' configuration with a bias-driven SOL current of  $I_{SOL} = 0.2kA$ .  $p_w$  and  $p_{w/o}$  represent the pressure computed by HINT with and without the biasing SOL current, respectively.  $p_{a_o}$  denotes the on-axis pressure of the equilibrium without biasing.

Fig. 4(a) shows the toroidally averaged pressure profiles at the midplane for various bias-driven SOL current amplitudes, ranging from 0 kA to 1 kA in 0.2 kA increments. In this work, the pressure is normalized by the on-axis pressure of the equilibrium without biasing unless otherwise specified. Away from resonant rational surfaces, the pressure profiles remain relatively unaffected by the increasing SOL current. While near the resonant surfaces where magnetic islands form, clear pressure flattening is observed. In the pedestal region, significant pressure reduction occurs as the magnetic field becomes stochastic. As SOL current amplitude increases, the pressure modification becomes more pronounced but not in a strictly linear manner. For instance, comparing Fig. 4(b) and (c), corresponding to  $I_{SOL} = 0.2$  kA and 0.4 kA respectively, reveals that while the color bar range in Fig. 4(c) is twice that of Fig. 4 (b), the blue regions indicating pressure reduction are noticeably deeper and broader, implying a nonlinear effect. As the SOL current approaches 1 kA, the resonance strength further increases, enhancing edge stochasticity and resulting in additional flattening and the onset of fluctuations in the pedestal pressure profile. Overall, as the SOL current increases, the pedestal height decreases, with a slight inward shift of the pedestal, particularly for the 0.8 kA and 1 kA cases. These nonlinear 3D MHD equilibria, characterized by

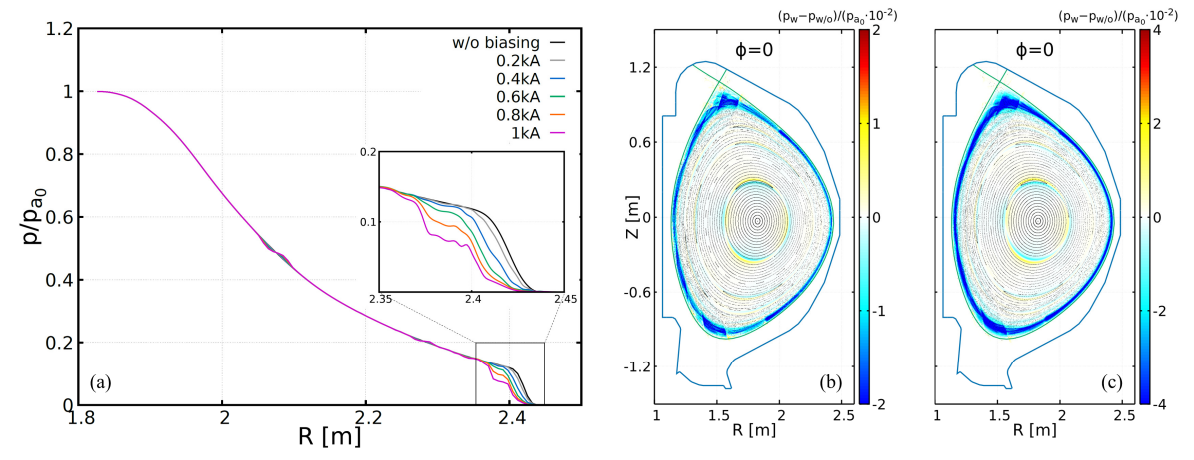


FIG. 4. (a) The toroidally averaged pressure profiles at the midplane for systematically varied bias-driven SOL current amplitudes, (b) and (c) the pressure modifications and Poincaré plots at  $\phi = 0$  for the '+ - + -' configuration with a bias-driven SOL current of  $I_{SOL} = 0.2$  kA and 0.4kA, respectively.

substantial modifications of the edge pressure gradient, are expected to strongly affect the characteristics and evolution of edge MHD instabilities.

## 3.3. Edge instability with biasing

Based on the 3D equilibria generated for various bias-driven SOL current amplitudes, the time evolution of MHD instabilities is investigated by solving the full set of MHD equations using the MIPS code. As shown in Fig. 5, the growth rate of instabilities, reflected by the slope of the curves during the linear phase, generally decreases with increasing SOL current. The evolution of total kinetic energy reveals a delayed onset of instability for most cases, except for the  $I_{\rm SOL}=0.6$  kA case. Although the growth rate in this case is slightly lower than that for  $I_{\rm SOL}=0.4$  kA, the earlier onset may be attributed to a slightly steeper pressure gradient near the pedestal foot, as indicated by the comparison between the green and blue curves in Fig. 4(a). At higher current levels ( $I_{\rm SOL}=0.8$  kA and 1 kA), the pedestal height is substantially reduced, leading to a further decrease in the instability growth rate. Since the MIPS code does not capture the full ELM cycle dynamics, all cases ultimately enter a nonlinear saturation phase, where the total kinetic energy levels off to similar values in logarithmic scale. Notably, when viewed in linear coordinates, the saturated kinetic energy decreases distinctly with increasing SOL current.

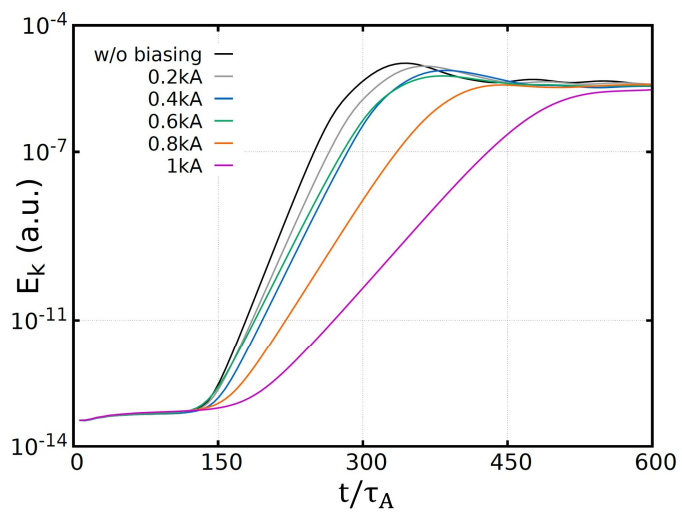


FIG. 5. Temporal evolution of the kinetic energy (logarithmic scale) of MHD instabilities for varying bias-driven SOL current amplitudes. Time is normalized to the Alfvén time.

To elucidate the instability dynamics, the evolution of mode structures is analysed using the perturbed pressure distribution and associated magnetic topology in cylindrical coordinates. Fig. 6 presents contour plots of the pressure perturbation at the  $\phi=0$  toroidal cross-section, comparing cases without biasing and with a bias-driven SOL current of 0.4 kA. In the natural ELM case (i.e. without biasing), a typical edge ballooning mode develops on the low-field side during the early linear phase ( $t=200\,\tau_A$ ). As the instability evolves ( $t=250\,\tau_A$ ), erosion of the edge magnetic surfaces is observed, and by the onset of the nonlinear phase ( $t=300\,\tau_A$ ), the mode transitions into an interchange-like structure superimposed with ballooning characteristics. With the application of biasing, the amplitude of edge instabilities is significantly reduced, as evidenced by the lower magnitude in the colour scale at corresponding time slices. Furthermore, the spatial distribution of the most unstable regions exhibits clear toroidal modulation induced by the applied n=2 dominant perturbation. This modulation is clearly evident when comparing the  $\phi=0$  and  $\phi=\pi/2$  cross-sections (Fig 6(b), (d) and (f), (h)): while the unstable regions remain similar in the natural ELM case, pronounced toroidal asymmetry appears in the biased case, indicating a coupling between the applied perturbation and the evolving edge mode structure.

To further characterize the instability dynamics, the temporal evolution of toroidal mode components of the kinetic energy is examined, as shown in Fig. 7. In the absence of biasing, high-n modes with the dominant mode at n=27 rapidly emerge during the early linear phase and remain dominant throughout as Fig. 8(a) shows. In contrast, with a bias-driven SOL current of 0.4 kA (Fig. 8(b)), the onset of high-n modes is noticeably delayed, while the evolution of low-n modes proceeds similarly to, or slightly earlier than that in the unbiased case. In the nonlinear saturation phase, the n=2 mode becomes dominant, indicating a redistribution of mode energy and reflecting the influence of the externally applied n=2 dominant perturbation on the instability spectrum. Fig. 7(c) shows the kinetic energy of individual toroidal mode components (n=1-32) at the saturation phase  $(t=600 \tau_A)$ . In the absence of biasing, the dominant mode is n=27, whereas for bias-driven SOL currents exceeding  $0.4 \, \text{kA}$ ,

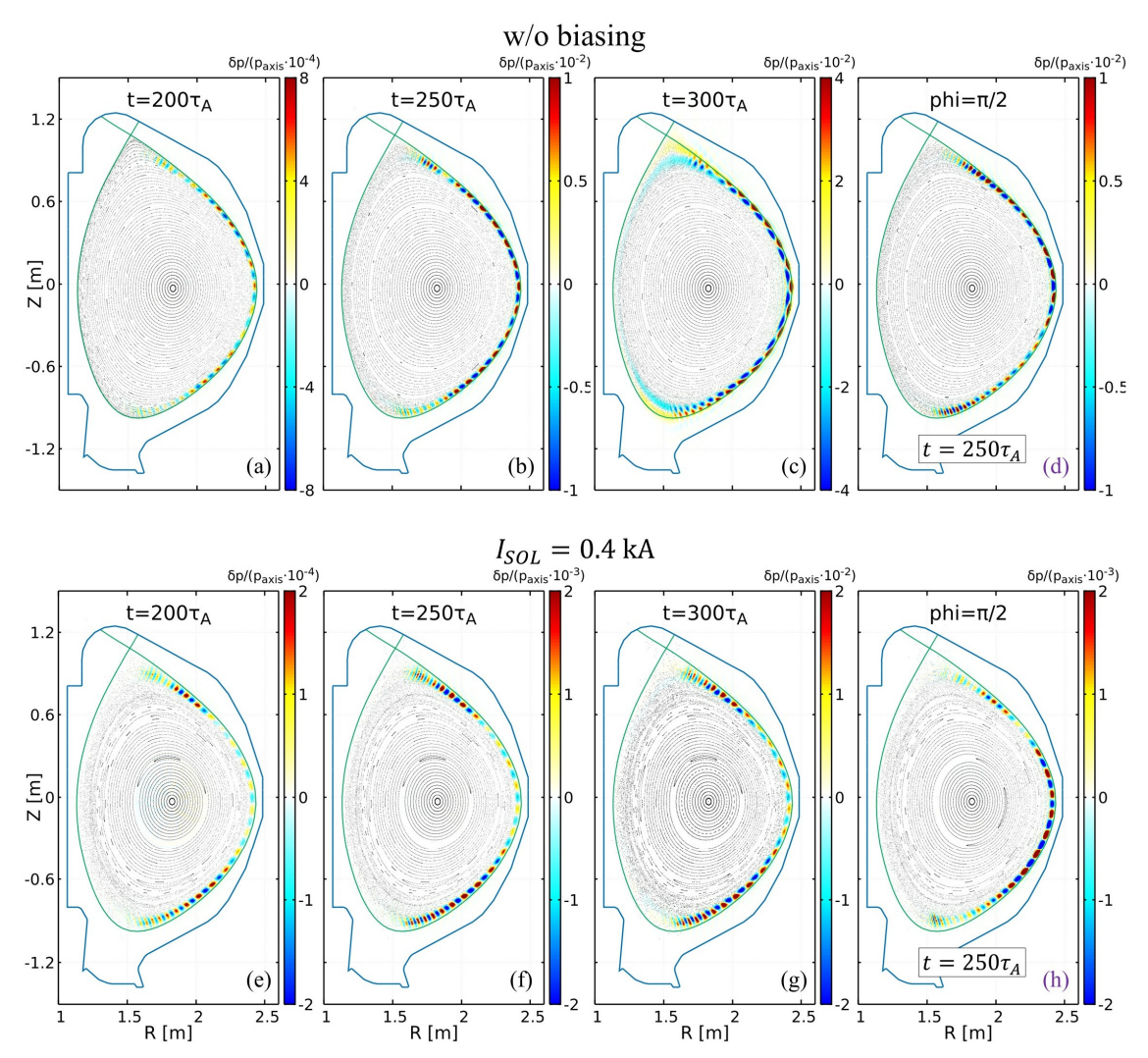


FIG. 6. Pressure perturbations at selected time slices for (a-c) unbiased and (e-g) biased ( $I_{SOL}=0.4$  kA) cases, shown at the  $\phi=0$  toroidal cross-section. Panels (d) and (h) show corresponding perturbations at  $\phi=\pi/2$  for t=250  $\tau_A$  (where  $\tau_A$  is the Alfvén time).

the peak energy shifts to n=2. This shift highlights the impact of the externally imposed n=2 dominant perturbation, which also enhances the energy content of even-n modes compared to adjacent odd-n components, particularly in the low-n range. Fig 7(d) summarizes the linear growth rates of individual toroidal mode components for different bias-driven SOL current amplitudes. In the natural ELM case, the low-n modes exhibit slightly higher growth rates than the high-n modes, despite their delayed onset, as they ultimately reach comparable amplitudes at nonlinear phase (see Fig. 7(a)). With the application of biasing, the growth rates of different n components tend to remain at a similar level. A general trend of decreasing growth rate with increasing SOL current is observed, except for the  $I_{\rm SOL}=0.4$  kA and 0.6 kA cases, which show nearly the same values. Given that the estimated bias-driven SOL current can reach up to 1.2 kA per electrode in HL-3, the numerical results presented here suggest that the proposed biasing configuration represents a promising approach for ELM control in HL-3 H-mode discharges with mega-ampere-level plasma currents.

## 4. CONCLUSION AND DISCUSSION

This study presents a numerical investigation of ELM dynamics under divertor biasing in HL-3 H-mode plasmas, using the 3D nonlinear HINT and MIPS codes. For a typical 1.6 MA H-mode discharge, the application of a biasdriven SOL current approaching 1 kA per plate as designed leads to a clear modification of pedestal pressure and edge stabilities. These changes are primarily attributed to restructuring of the edge magnetic topology with resonant magnetic field, resulting in reduced pedestal pressure gradient and altered ELM behaviour. The findings demonstrate that the proposed biasing configuration may serve as an effective strategy for ELM control in HL-3.

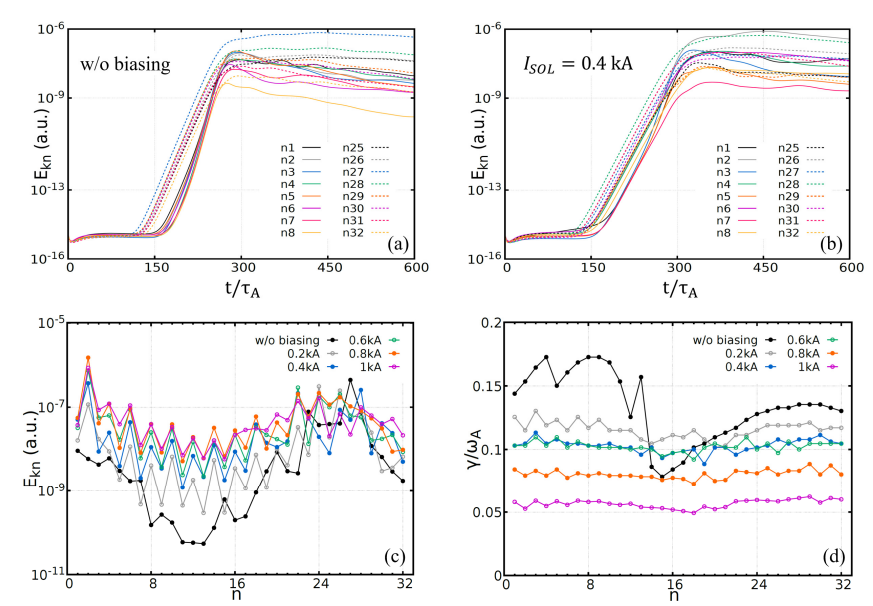


FIG.7. Temporal evolution of toroidal mode-decomposed kinetic energy (logarithmic scale) for (a) unbiased and (b) biased ( $I_{SOL} = 0.4 \text{ kA}$ ) cases. (c) Kinetic energy at  $t = 600 \tau_A$  and (d) growth rates for individual toroidal mode components under varying amplitudes of bias-driven SOL current.

The spectral properties of the biasing-induced magnetic perturbations are analysed and found to differ from those generated by conventional 3D RMP coils. The biasing system preferentially excites resonant components with minimal non-resonant content. Furthermore, bias-driven SOL currents aligned along magnetic field lines closer to the pedestal region than RMP coils and with helicities matching the resonant surfaces can generate comparable edge perturbations with lower total current, thereby potentially minimizing the impact on the core plasma.

The 3D equilibria computed with increasing bias-driven SOL current amplitudes reveal a nonlinear response of the plasma edge, characterized by enhanced magnetic stochasticity and pressure profile modification at higher current levels. These changes are self-consistently balanced by the plasma to maintain MHD force balance. Under experimental conditions, additional complexities may arise due to the finite area of the biased targets, self-induced perturbations of the currents along flux tubes and potential SOL current leakage. A more rigorous simulation of SOL current behaviour under biasing would ideally employ a particle-in-cell (PIC) approach, which demands substantial computational resources. In the present study, a simplified model using a single filament with constant current density per biased plate is employed. Despite its simplicity, this approach successfully captures the essential features of the magnetic topology and edge stochasticity, as the helical structure of field lines remains largely preserved even within stochastic regions. This supports the validity of the model for predictive studies of edge behaviour under SOL current biasing.

MHD stability analysis using the MIPS code shows that in the absence of biasing, high-n ballooning modes emerge early and remain dominant throughout both the linear and nonlinear phases. When biasing is applied, the onset of high-n modes is delayed, and the growth rates of all toroidal components are systematically reduced with increasing SOL current. In the nonlinear regime, the externally imposed perturbation redistributes mode energy, leading to a marked enhancement of the n=2 component consistent with the dominant biasing configuration. These findings suggest that the biasing scheme not only suppresses linear growth but also alters the nonlinear dynamics of edge instabilities through mode coupling.

The achievable SOL current amplitude and its effective path length are influenced by multiple factors, including SOL plasma conditions such as density and temperature, as well as parallel and cross-field transport and the connection length of open magnetic field lines. It should also be noted that plasma flow-induced screening effects are not considered in the present study. These effects may reduce the degree of edge stochasticity and magnetic island widths Accurate comparison with experimental data, particularly in validating the SOL current amplitudes and assessing the impact of screening, is essential. Future work will address these aspects by combining experimental observations with resistive MHD response modelling using the MARS-F code.

#### **ACKNOWLEDGEMENTS**

This work was supported by the National Magnetic Confinement Fusion Energy R&D Program (Nos. 2022YFE03060002 and 2019YFE03030003), the Youth Science and Technology Innovation team of Sichuan Province (No. 2022JDTD0003), the National Natural Science Foundation of China (Nos. 12375214 and 12475218), the China National Nuclear Corporation Fundamental Research Program (Nos. CNNC-JCYJ-202236 and CNNC-JCYJ-202324), and the Innovation Program of Southwestern Institute of Physics (No. 202301XWCX006-04). Most of the numerical computations were carried out on the Tianhe supercomputing system at the National Supercomputer Centre in Tianjin, China.

#### REFERENCES

- [1] Wagner, F. et al. Regime of Improved Confinement and High Beta in Neutral-Beam-Heated Divertor Discharges of the ASDEX Tokamak. Phys. Rev. Lett. **49** (1982) 1408.
- [2] Kirk, A. et al. Spatial and Temporal Structure of Edge-Localized Modes. Phys. Rev. Lett. 92 (2004) 245002.
- [3] Igochine, V. Physics of resistive wall modes. Nucl. Fusion 52 (2012) 074010.
- [4] King, J. D. et al. Hybrid-like 2/1 flux-pumping and magnetic island evolution due to edge localized mode-neoclassical tearing mode coupling in DIII-D. Phys. Plasmas 19 (2012) 022503.
- [5] Loarte, A. et al. Power and particle control. Nucl. Fusion 47 (2007) S203.
- [6] Evans, T.E. et al. Edge stability and transport control with resonant magnetic perturbations in collisionless tokamak plasmas. Nat. Phys. 2 (2006) 419.
- [7] Evans, T.E. et al. Suppression of Large Edge-Localized Modes in High-Confinement DIII-D Plasmas with a Stochastic Magnetic Boundary. Phys. Rev. Lett. **92** (2004) 235003.
- [8] Liang, Y. et al. Active Control of Type-I Edge-Localized Modes with n = 1 Perturbation Fields in the JET Tokamak. Phys. Rev. Lett. **98** (2007) 265004.
- [9] Kirk, A. et al. Resonant magnetic perturbation experiments on MAST using external and internal coils for ELM control. Nucl. Fusion **50** (2010) 034008.
- [10] Suttrop, W. et al. First Observation of Edge Localized Modes Mitigation with Resonant and Nonresonant Magnetic Perturbations in ASDEX Upgrade. Phys. Rev. Lett. **106** (2011) 225004.
- [11] Jeon, M.Y. et al. Suppression of Edge Localized Modes in High-Confinement KSTAR Plasmas by Nonaxisymmetric Magnetic Perturbations. Phys. Rev. Lett. **109** (2012) 035004.
- [12] Sun, Y. et al. Nonlinear Transition from Mitigation to Suppression of the Edge Localized Mode with Resonant Magnetic Perturbations in the EAST Tokamak. Phys. Rev. Lett. **117** (2016) 115001.
- [13] Bécoulet, M. et al. Numerical study of the resonant magnetic perturbations for Type I edge localized modes control in ITER. Nucl. Fusion 48 (2008) 024003.
- [14] Snyder, P. B. and Wilson, H. R. Ideal magnetohydrodynamic constraints on the pedestal temperature in tokamaks. Plasma Phys. Control. Fusion **45** (2003) 1671.
- [15] Hao, G.Z. et al. Toroidal modeling of 3D perturbations generated by current filaments in scrape-off layer in tokamak with biased divertor targets. Nucl. Fusion **63** (2023) 016006.
- [16] Huysmans, G.T.A. and Czarny, O. MHD stability in X-point geometry: simulation of ELMs. Nucl. Fusion 47 (2007) 659.
- [17] Xu, X.Q. et al. Nonlinear Simulations of Peeling-Ballooning Modes with Anomalous Electron Viscosity and their Role in Edge Localized Mode Crashes. Phys. Rev. Lett. **105** (2010) 175005.
- [18] Park, W. et al. Plasma simulation studies using multilevel physics models. Phys. Plasmas 6 (1999) 1796.
- [19] Sovinec, C.R. et al. Nonlinear magnetohydrodynamics simulation using high-order finite elements. J. Comput. Phys. **195** (2004) 355.
- [20] Todo, Y. et al. Linear and nonlinear particle-magnetohydrodynamic simulations of the toroidal Alfvén eigenmode. Phys. Plasmas 5 (1998) 1321.
- [21] Todo, Y. et al. Simulation Study of Ballooning Modes in the Large Helical Device. Plasma Fusion Res. 5 (2010) S2062.
- [22] Suzuki, Y. HINT modeling of three-dimensional tokamaks with resonant magnetic perturbation. Plasma Phys. Control. Fusion 59 (2017) 054008.
- [23] Meneghini, O. et al. Integrated modeling applications for tokamak experiments with OMFIT. Nucl. Fusion 55 (2015) 083008.